JGP Journal of General Physiology

RESEARCH ARTICLE

A channel profile report of the unusual K^+ channel KtrB

Vedrana Mikušević[1], Marina Schrecker[1], Natalie Kolesova[1], Miyer Patiño-Ruiz[2], Klaus Fendler[2], and Inga Hänelt[1]

KtrAB is a key player in bacterial K^+ uptake required for K^+ homeostasis and osmoadaptation. The system is unique in structure and function. It consists of the K^+-translocating channel subunit KtrB, which forms a dimer in the membrane, and the soluble regulatory subunit KtrA, which attaches to the cytoplasmic side of the dimer as an octameric ring conferring Na^+ and ATP dependency to the system. Unlike most K^+ channels, KtrB lacks the highly conserved T(X)GYG selectivity filter sequence. Instead, only a single glycine residue is found in each pore loop, which raises the question of how selective the ion channel is. Here, we characterized the KtrB subunit from the Gram-negative pathogen *Vibrio alginolyticus* by isothermal titration calorimetry, solid-supported membrane–based electrophysiology, whole-cell K^+ uptake, and ACMA-based transport assays. We found that, despite its simple selectivity filter, KtrB selectively binds K^+ with micromolar affinity. Rb^+ and Cs^+ bind with millimolar affinities. However, only K^+ and the poorly binding Na^+ are efficiently translocated, based on size exclusion by the gating loop. Importantly, the physiologically required K^+ over Na^+ selectivity is provided by the channel's high affinity for potassium, which interestingly results from the presence of the sodium ions themselves. In the presence of the KtrA subunit, sodium ions further decrease the Michaelis–Menten constant for K^+ uptake from milli- to micromolar concentrations and increase the V_{max}, suggesting that Na^+ also facilitates channel gating. In conclusion, high binding affinity and facilitated K^+ gating allow KtrAB to function as a selective K^+ channel.

Introduction

K^+ is the most abundant intracellular cation of almost all living organisms. Maintaining its distribution across the cell membrane is pivotal for a normal cell function (Williams and Wacker, 1967). In bacteria, the balance of K^+ is essential for pH homeostasis, osmoadaptation (Epstein, 2003), and electrical signaling in biofilms (Prindle et al., 2015). To fulfill the different requirements, a variety of high- and low-affinity K^+ transport systems is found side by side (Holtmann et al., 2003; Lundberg et al., 2013; Diskowski et al., 2015; Gundlach et al., 2017). The most important players in bacterial osmoadaptation are KtrAB, TrkAH, and KdpFABC (Epstein, 2003; Holtmann et al., 2003; Diskowski et al., 2015). Of those the three subunits, KtrB, TrkH, and KdpA are members of the so-called superfamily of K^+ transporters. While KdpFABC is a primary active K^+ transporter, which ensures survival under K^+ limitation, the other two are ion channels crucial for maneuvering bacteria through everyday challenges. The ion-translocating subunits KtrB and TrkH consist of four fused M1-P-M2 motifs, called D1 to D4, which organize around a pseudo fourfold symmetry axis providing the ion permeation pathway (Cao et al., 2011; Vieira-Pires et al., 2013). Uniquely, both proteins form functional homodimers in the plasma membrane, which assemble with their respective cytoplasmic regulatory proteins, KtrA and TrkA. The cytoplasmic proteins belong to the regulator of K^+ conductance proteins and control ion gating in a nucleotide- and Na^+- (KtrA) or H^+- (TrkA) dependent manner (Bakker and Mangerich, 1983; Tholema et al., 1999; Kröning et al., 2007; Cao et al., 2013). In the absence of the regulatory subunits, KtrB and TrkH are still active. Single-channel recordings of TrkH showed a fourfold increased open probability compared with TrkAH, suggesting that the regulatory subunits are required to efficiently close the channels (Cao et al., 2013).

The single-channel recordings also allowed accessing the ion selectivity of TrkAH. Similar conductivities were measured for K^+, Rb^+, and Cs^+, while Na^+ and Li^+ conducted with significantly slower rates. The weak selectivity was assumed to be in agreement with the poorly conserved selectivity filter found in both TrkH and KtrB. Instead of the canonical selectivity filter sequence T(X)GYG (Doyle et al., 1998), only the first glycine residue in each P-loop is conserved (compare Fig. 1). Not further examined were the open probabilities in

[1]Institute of Biochemistry, Goethe University Frankfurt, Frankfurt, Germany; [2]Department of Biophysical Chemistry, Max Planck Institute for Biophysics, Frankfurt, Germany.

Correspondence to Inga Hänelt: haenelt@biochem.uni-frankfurt.de.

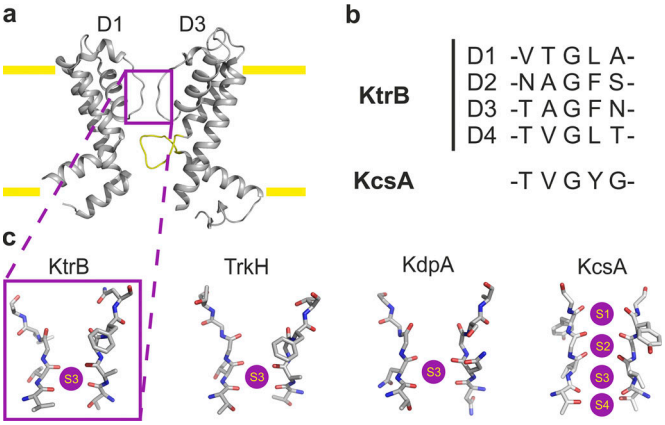

Figure 1. **Ion permeation pathway and selectivity filter. (a)** Ribbon representation of one KtrB protomer (4J7C) highlighting the permeation pathway with the selectivity filter (purple box) and the intramembrane loop (yellow). Domains D1 and D4 in the front and the back were removed for clarity. **(b)** Selectivity filter signature sequence of all four KtrB domains from *V. alginolyticus* in comparison with the signature sequence of KcsA. **(c)** Stick representations of the selectivity filters of KtrB (4J7C), TrkH (4J9U), KdpA (5MRW), and KcsA (1BL8) shown with the so far confirmed K^+ binding sites as purple spheres. Domains D2 and D4 of KtrB, TrkH, and KdpA, and two subunits of KcsA, respectively, were removed for clarity.

dependence of the different tested cations; thus, the efficiency of ion translocation remains unknown. In KtrB and TrkH, the pores are restricted by an intramembrane loop formed by the central part of D3M2, which is located directly below the selectivity filter and functions as a molecular gate (Hänelt et al., 2010a; Cao et al., 2013; Vieira-Pires et al., 2013). The intramembrane loop is controlled by the regulatory subunits KtrA and TrkA, respectively (Kröning et al., 2007; Cao et al., 2013; Vieira-Pires et al., 2013; Levin and Zhou, 2014; Szollosi et al., 2016; Diskowski et al., 2017). Earlier studies on KtrB showed that the molecular gate limits the uptake velocity for K^+ but does not seem to affect K^+ affinity or the translocation of Na^+ (Hänelt et al., 2010a). Thus, the intramembrane loop may have different effects on the translocation of different cations, favoring one over another.

For KtrAB, a detailed characterization of the ion selectivity and translocation was missing. To address both, we here applied isothermal titration calorimetry (ITC), solid-supported membrane (SSM)–based electrophysiology, and a 9-amino-6-chloro-2-methoxyacridine (ACMA)–based flux assay using detergent-purified or liposome-reconstituted KtrB from *Vibrio alginolyticus* as well as whole-cell uptake experiments. Surprisingly, these measurements uncovered a channel profile for KtrB that is significantly different from its homologue, TrkH.

Materials and methods

Protein production and purification

Escherichia coli strain LB2003 (F^- *thi metE rpsL gal rha kup1 ΔkdpABC5 ΔtrkA*; Stumpe and Bakker, 1997) was used for the overexpression of genes *ktrB-his*$_6$ and *ktrB*$_{G316S}$*-his*$_6$ encoded on the plasmids pEL903 and pEL903-G316S (Tholema et al., 2005; Hänelt et al., 2010a), respectively. 12-liter cultures of LB2003/pEL903 and LB2003/pEL903-G316S were grown in K3 minimal medium containing 0.2% glycerol and 100 µg/ml ampicillin as a selection marker and induced with 0.02% L-arabinose. Since the strain lacks all endogenous K^+ uptake systems, cell growth under potassium limitation ensured the functionality of the produced protein (Stumpe and Bakker, 1997). Cells were harvested after reaching the late-exponential growth phase. All cells were washed and resuspended in buffer S (420 mM NaCl, 180 mM KCl, and 50 mM Tris-HCl, pH 8) supplemented with 100 µM of the serine protease inhibitor PMSF, 300 µM benzamidine, 1 mM EDTA, and a spatula of DNase I (Sigma-Aldrich). Cells were lysed by sonication (Branson Sonifier), and the suspension was subjected to a low-speed centrifugation step at 15,000 *g* for 15 min at 4°C, followed by an overnight centrifugation of the supernatant at 100,000 *g*. The membrane pellet was homogenized and resuspended in buffer S with protease inhibitors to a protein concentration of 10 mg/ml, as determined by bicinchoninic acid assay using a kit (Thermo Fisher Scientific). For solubilization, 1% β-D-dodecylmaltoside (DDM) was added to the membrane suspension and incubated for 1 h under gentle agitation. Nonsoluble proteins were removed by centrifugation at 200,000 *g* for 30 min at 4°C. The supernatant was incubated with nickel–nitrilotriacetic acid–agarose resin for 1 h at 4°C in the presence of 10 mM imidazole. The nickel–nitrilotriacetic acid–agarose resin was transferred to a gravity flow column and washed with 100 column volumes of buffer W (140 mM NaCl, 60 mM KCl, and 20 mM Tris-HCl, pH 8) with 0.04% DDM and 50 mM imidazole. KtrB-His$_6$ or KtrB$_{G316S}$-His$_6$ was eluted from the column with buffer W containing 0.04% DDM and 500 mM imidazole. The eluted protein was concentrated to 500 µl with a 50 MWCO Centriprep (Merck Millipore) for size-exclusion chromatography. For the final purification step, a size-exclusion chromatography was performed using a Superdex Increase 200 10/300 GL column (GE Healthcare) equilibrated to either buffer W containing 0.04% DDM or the ITC buffers (200 mM choline-Cl or 200 mM LiCl, 0.04% DDM, and 20 mM Tris-HCl, pH 7). Coomassie staining after SDS-PAGE determined the purity of the sample.

ITC

ITC measurements were performed at 24°C with a MicroCal iTC200 System (GE). KtrB-His$_6$ at a concentration of ∼2.5 mg/ml was in ITC buffer. The titration solution consisted of ITC buffer, in which either choline-Cl or LiCl was replaced by the indicated concentrations of LiCl, NaCl, KCl, RbCl, or CsCl to assure isoosmotic conditions. A volume of 2 or 1.5 µl was used for each injection, with the exception of the first injection, which was adjusted to 0.2 µl. Measurements involved 19–26 injections with 3-min intervals in between each injection and a reference power of 11.0 µcal/s. All titrations were analyzed by MicroCal ITC-ORIGIN Analysis Software. The heat of dilution acquired from injecting a ligand into buffer was subtracted before data fitting.

Reconstitution into liposomes

E. coli polar lipids were extracted from *E. coli* total lipid extract (Avanti; Driessen and Konings, 1993). Vesicles were formed by resuspending a dried lipid film in 50 mM potassium phosphate

buffer, pH 7.0, to a lipid concentration of 10 mg/ml (wt/wt). Lipids were flash frozen and stored at −80°C until use. Subsequently, liposomes were thawed, spun down, and resuspended in either SSM buffer (300 mM choline-Cl, 50 mM Tris, 50 mM MES, 50 mM HEPES, and 5 mM $MgCl_2$, pH 7.5) or ACMA buffers (150 mM NaCl, KCl, RbCl, or CsCl with 20 mM HEPES, pH 7.35). Liposomes were flash frozen three times and slowly thawed before reconstitution.

Purified KtrB-His_6 or variant $KtrB_{G316S}$ was reconstituted into *E. coli* polar lipid liposomes according to an established protocol (Hänelt et al., 2010b). Proteoliposomes with lipid to protein ratios (LPR) of 5:1 and 100:1 (wt/wt) were generated for SSM-based electrophysiology and ACMA-based flux assay, respectively. In brief, after extrusion through a 400-nm filter, the liposomes were set to a concentration of 4 mg/ml in their respective buffers. Subsequently, 10% Triton X-100 was titrated to the liposomes until reaching the point slightly after the detergent saturation limit by following the absorption at 540 nm (Geertsma et al., 2008). The corresponding amount of protein (or buffer for control liposomes) was added to the destabilized liposomes following a series of BioBead additions according to the existing protocol (Hänelt et al., 2010b). Finally, the proteoliposomes were washed two times with their respective buffers. They were either immediately used for the ACMA assay or aliquoted and flash-frozen for SSM-based electrophysiology.

SSM-based electrophysiology

Preparation of the gold electrodes was done according to an existing standard protocol (Bazzone et al., 2013). Upon contact of the sensor with an aqueous solution of 100 mM potassium phosphate buffer, pH 7, a hybrid bilayer of phosphatidylcholine (PC) with octadecylamine was formed, resulting in a functionalized SSM sensor module. As reference, an Ag/AgCl electrode was used, separated from the main fluid pathway by an agarose gel bridge. The SSM sensor module was connected to a current amplifier set to a gain of 10^9 V/A and the reference electrode to the function generator (Schulz et al., 2008). To ensure the quality of the SSM sensor, the conductance and capacitance were measured. The parameters for a conductance between 0.1 and 0.3 nS and a capacitance of 2–3.5 nF were considered acceptable for a sensor size of 1 mm (Bazzone et al., 2013).

A total of 32 µl of a proteoliposome/control liposome suspension with a lipid concentration of 2–5 mg/ml was sonicated (3 × 10-s intervals) and applied to the SSM followed by an incubation period of 2–3 h, allowing the adsorption of the liposomes and thereby the formation of the sensor element.

All SSM solutions were buffered with 50 mM Tris, 50 mM MES, 50 mM HEPES, 5 mM $MgCl_2$, 200 mM choline-Cl, and 100 mM of different chloride salts at pH 7.5. To induce transient currents, a solution exchange protocol was performed, switching from a nonactivating (NA) solution to an activating (A) solution and back (NA-A-NA), with each step lasting for 0.5 s. The A solution contained additionally 100 mM of chloride salts mixed from *x* mM choline-Cl with *y* mM of LiCl, NaCl, KCl, RbCl, or CsCl in different combinations (see Table S1). Transient currents shown in one graph always resulted from one set of measurements recorded on the same sensor element. Peak currents from each set of measurement were normalized to the highest respective peak current to allow data averaging. The time-dependent stability of protein activity was monitored during a series of measurements. Therefore, the current for the same A solution was measured at the beginning and end of each series, and the peak currents were compared. A rundown of <15% was considered to be within the acceptable range. A linear rundown was presumed and mathematically corrected using the formula for the correction factor:

$$F = \frac{I_i}{I_i - (I_i - I_f)\frac{t}{t_f}}. \quad (1)$$

Here, I_i corresponds to the initial current, and I_f corresponds to the final current at the end of each series of measurements. t describes the relative time of every individual measurement and t_f the duration of the whole series of measurement. The measured currents are multiplied with the correction factor F.

ACMA assay

10 µl of liposomes in the indicated ACMA buffer (10 mg/ml, LPR 100:1) were added to 190 µl of outside buffer (20 mM HEPES-ethanolamine, pH 7.3, 150 mM LiCl, and 2 µM of the pH-sensitive dye ACMA) in a fluorescence cuvette. Fluorescence was monitored at an excitation wavelength of 410 nm and an emission wavelength of 500 nm (2-nm bandwidths). After a stable fluorescence signal was reached, 1 µM of the H^+ ionophore carbonyl cyanide-m-chlorophenylhydrazone (CCCP) was added and quickly mixed, which abolished any established membrane potential. Consequently, ACMA quenching by H^+, which permeated through CCCP into the liposomes, was determined to indirectly measure the efflux of cations through KtrB or variant $KtrB_{G316S}$ (Su et al., 2016). Finally, the maximally possible ACMA quenching was determined by the addition of either 20 nM valinomycin (Val) for vesicles containing KCl, RbCl, or CsCl or 5 µM sodium ionophore IV (Selectophore by Sigma-Aldrich) for vesicles containing NaCl. Fluorescence traces were normalized to the initial signals before CCCP addition. Evaluation of fluorescence changes and decay rates was done with OriginPro 2017.

K^+ uptake into whole cells

Depletion of the cells from alkali cations and net K^+ uptake by K^+- and Na^+-depleted LB2003 cells was performed as described by Tholema et al. (2005), except that LB2003 was suspended in 200 mM triethanolamine/HEPES, pH 7.5, to add cations in the defined concentrations.

Online supplemental material

Fig. S1 shows a purification profile of KtrB and its reconstitution efficiency into liposomes. Fig. S2 presents the ITC measurement determining the apparent affinity for K^+ in the presence of 200 mM NaCl. Fig. S3 summarizes the principles of SSM-based electrophysiology, while Fig. S4 compares the artificial currents measured with control liposomes with the transient currents attributed to KtrB-containing liposomes. Table S1 summarizes all buffers used for SSM-based electrophysiology measurements.

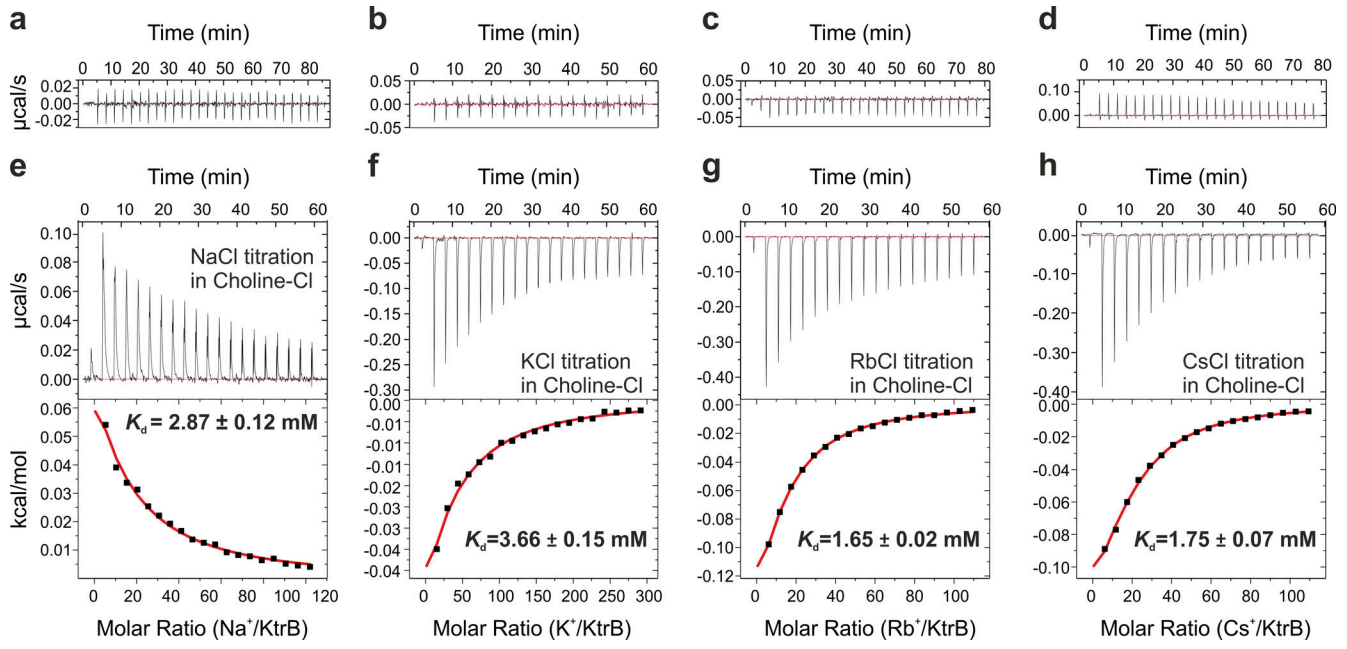

Figure 2. **Binding affinity of monovalent cations to KtrB examined by ITC. (a–d)** Cation to buffer control titrations are shown above each (e–h) cation to protein titration. For the cation to protein titrations, the upper panels show the raw heat exchange data, associated with Na^+ (e), K^+ (f), Rb^+ (g), or Cs^+ (h) binding to detergent-solubilized KtrB in 200 mM choline-Cl buffered with 20 mM Tris-HCl, pH 7.5. The lower panels giving the integrated injection heat pulses, normalized per mole of injection, reveal different binding curves fitted by one-site binding model. Individual K_d values derived from fitting ± standard error (SE) are indicated. Each graph represents an example of three independent experiments. Mean data ± SEM are summarized in Table 1.

Results

KtrB shows selective ion binding in the presence of small cations

To investigate the ion binding of KtrB, *ktrB-his*$_6$ from *V. alginolyticus* was heterologously expressed in and KtrB purified from *E. coli* strain LB2003 (Stumpe and Bakker, 1997; Fig. S1 a). To determine the equilibrium K_d of different cations to KtrB, ITC experiments were performed with detergent-purified protein. Cation to buffer control titrations are shown in Fig. 2, a–d. Titration experiments with KtrB in choline-Cl-based buffers resulted in very similar binding affinities in the range of 1.6 to 2.9 mM (Fig. 2, e–h; and Table 1) with regard to four of the five tested cations (Na^+, K^+, Rb^+, and Cs^+), while no binding was observed for Li^+ (data not shown). In contrast to that, the determined binding enthalpies revealed clear differences: while the binding of K^+, Rb^+, and Cs^+ was strongly exothermic, the binding of Na^+ was endothermic (compare Fig. 2, e and f–h) and reflected the high energy required for Na^+ dehydration upon binding to KtrB. We assumed that the wide-open and simple-fashioned selectivity filter allows for this fairly unselective binding (Fig. 2, a–d; and Table 1). However, all these measurements were performed in almost the complete absence of small cations, while it is known for KcsA that small cations are required to stabilize the protein's integrity (Krishnan et al., 2005). Further, under physiological conditions, usually mixed ion species are present.

Since no Li^+ binding to KtrB was determined in the above-mentioned experiments, we repeated all ITC measurements by substituting the choline-Cl-based with a LiCl-based buffer. Interestingly, with the modified condition, a significantly different ion binding profile of KtrB was determined (Fig. 3, e–h). While the apparent affinities for Rb^+ and Cs^+ remained similar (Fig. 3, g and h; and Table 1), no binding of Na^+ could be detected (Fig. 3 e and Table 1). In contrast, the apparent K_d value for K^+ decreased from 2.9 mM to ∼91 µM (compare Fig. 2 f, Fig. 3 f, and Table 1). Interestingly, even the presence of just 5 mM NaCl in the choline-Cl-based buffer was sufficient to induce a dramatic increase of binding affinity of KtrB to K^+ with a K_d value of 260 µM (Fig. 4 a). In conclusion, the presence of small cations significantly increases the binding affinity of KtrB to K^+, resulting in an at least 10 times higher selectivity for potassium over all other cations. These data suggest that small ions modulate the architecture of the selectivity filter.

The relatively low ion binding affinities for Rb^+, Cs^+, and Na^+ may indicate that the ion binding takes place not within the selectivity filter but in the cavity. The Na^+ binding, which was only measured in the absence of Li^+, may even reflect the proposed binding of small, modulatory cations, which lead to the stabilization of the selectivity filter and the increased affinity toward potassium ions. Therefore, we tested whether K^+ competes with the other ions and determined its apparent binding affinity in the presence of 50 mM NaCl, RbCl, and CsCl, respectively. In the presence of 50 mM NaCl, the affinity for K^+ only decreased to an apparent K_d of 1.8 mM, and even in the presence of 200 mM NaCl, the apparent K_d for K^+ was still 3.5 mM (Fig. 4 b and Fig. S2). Rb^+ and Cs^+ completely prevented K^+ binding to KtrB (Fig. 4, c and d). Thus, all ions appear to bind to the same or overlapping binding sites. However, Na^+ seems to bind with a comparably low affinity, which is why we still could determine a low apparent binding affinity for K^+ in the presence of 200 mM NaCl.

Table 1. **Biophysical parameters of ion binding to and translocation through KtrB**

ITC				ACMA	SSM	
Ion	**r (Å)**	**$K_d^{choline}$ (mM)**	**$K_d^{lithium}$ (mM)**	**H^+ flux**	**K_m (mM)**	**τ (ms)**
Li^+	0.60	nd	–		nd	nd
Na^+	0.95	1.8 ± 0.4	nd	+++	35.5 ± 1.9	45.2 ± 3.0
K^+	1.33	2.9 ± 0.3	0.091 ± 0.012	++	16.4 ± 1.8	15.2 ± 2.9
Rb^+	1.48	1.9 ± 0.1	2.4 ± 0.2	+	5.9 ± 0.6	8.3 ± 0.5
Cs^+	1.69	1.6 ± 0.1	1.7 ± 0.3	–	2.1 ± 0.3	9.2 ± 2.3

The ionic radii r are shown in Å (Hille, 2001). ITC: K_d values were obtained from a fit to a single binding isotherm (n = 3). ACMA: H^+ flux is ranked from best (+++) to worst (–) for each ion. SSM: K_m values obtained from the peak currents measured with SSM-based electrophysiology (n = 3 or 4). The decay times of the transient currents are indicated as τ, which were obtained from one-phase exponential decay fits (n = 3). nd, Not detectable. All errors are given as ±SEM.

Ion translocation through KtrB

Ion binding is a prerequisite for translocation but not a warranty. Here, we established SSM-based electrophysiology measurements with KtrB-containing liposomes with the aim to distinguish between the events of ion binding and ion translocation. With an efficiency of 80%, KtrB was reconstituted into liposomes (Fig. S1 b). In the SSM-based electrophysiological measurements, information about ion binding and translocation of KtrB was obtained from transient currents recorded upon concentration jumps. For this purpose, experiments were constructed as follows: an NA solution and an A solution were sequentially directed through the SSM cuvette in a 1.5-s NA (0.5 s)–A (0.5 s)–NA (0.5 s) solution exchange protocol (Fig. S3, a and b). For each measurement, signals obtained from the in parallel–prepared control liposomes (eLS) were subtracted (Fig. S4, a–e). These artifacts arise from interactions of cations with the lipid head groups (Garcia-Celma et al., 2007). Subsequently, the peak values and the decay times of the transient currents attributed to KtrB were determined and analyzed. Concentration jump measurements were performed with Li^+, Na^+, K^+, Rb^+, and Cs^+. While Li^+ did not result in transient currents bigger than the artifacts, increasing peak currents were recorded for the other four cations at increasing ion concentrations in otherwise iso-osmotic solutions (Fig. 5 and Fig. S4).

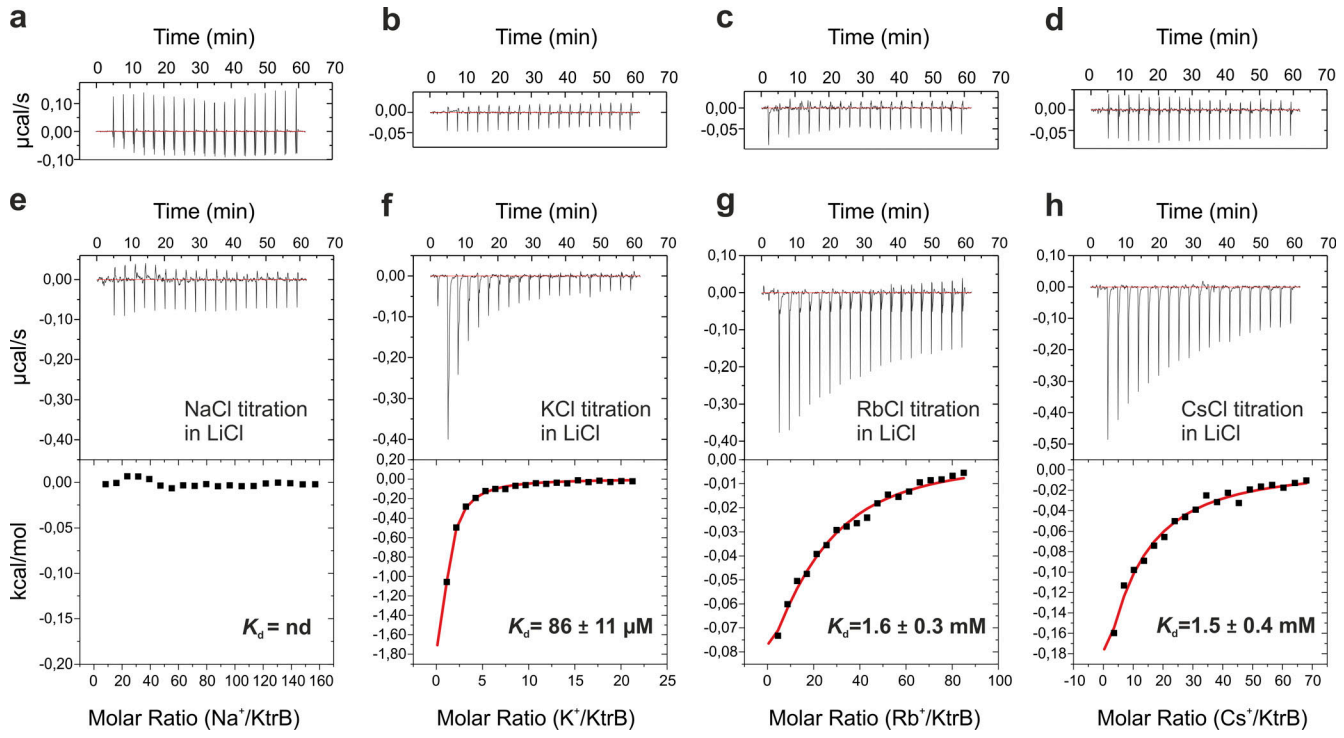

Figure 3. **Binding affinity of monovalent cations to KtrB examined by ITC. (a–d)** Cation to buffer control titrations are shown above each (e–h) cation to protein titration. For the cation to protein titrations, the upper panels show the raw heat exchange data, associated with Na^+ (e), K^+ (f), Rb^+ (g), or Cs^+ (h) binding to detergent-solubilized KtrB in 200 mM LiCl buffered with 20 mM Tris-HCl, pH 7.5. The lower panels giving the integrated injection heat pulses, normalized per mole of injection, reveal different binding curves fitted by one-site binding model. Individual K_d values derived from fitting ± SE are indicated. Each graph represents an example of three independent experiments. Mean data ± SEM are summarized in Table 1.

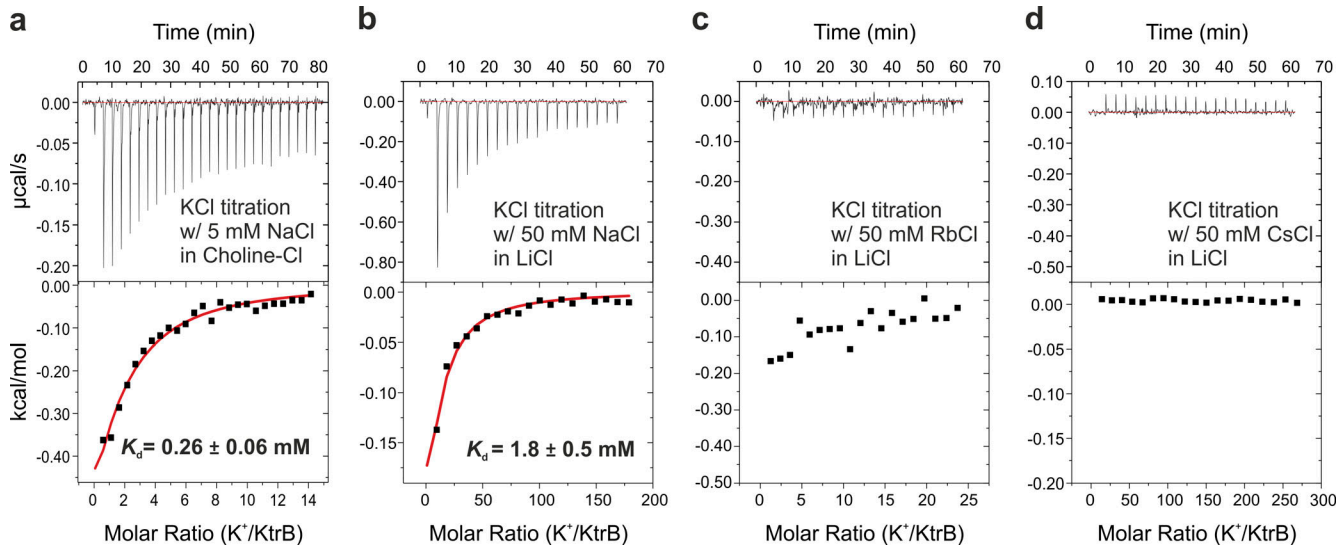

Figure 4. **K⁺ binding competition examined by ITC.** Potassium to protein titration in the presence of different cations. **(a)** KCl titration to protein solution in 195 mM choline-Cl with 5 mM NaCl reveals an apparent K_d of 0.26 mM. **(b–d)** KCl titration to protein solutions that contain 50 mM NaCl, RbCl, or CsCl in 150 mM LiCl solution buffered with 20 mM Tris-HCl, pH 7.5. The lower panels giving the integrated injection heat pulses, normalized per mole of injection, reveal different binding curves fitted by one-site binding model. Individual K_d values derived from fitting ± SE are indicated. Each graph represents an example of three independent experiments.

Comparing the peak currents from 100-mM concentration jumps shows a clear ion size dependency with the highest peak current for the biggest cation, Cs^+ (Fig. 5, a and b). However, when evaluating the normalized electrical charges (Fig. 5 c), which resulted from integrals of the peak currents, higher values for Na^+ and K^+ were acquired, suggesting that these two ions are actually better translocated than Rb^+ and particularly Cs^+. In agreement with this conclusion were the determined decay times ($\tau = t_1 ln(2)$). Usually fast decay times (τ) like in the case of Cs^+ (~9 s) and Rb^+ (~8 s) suggest pre–steady-state charge displacements (Table 1), corresponding to either a fast translocation or only a binding event, while slow decay times represent steady-state ion translocations (Bazzone et al., 2016, 2017). We determined decay times of K^+ and Na^+ currents of ~15 s and ~45 s, respectively (Table 1).

Establishing the Michaelis-Menten constant K_m for the different ions should further help to distinguish between ion binding and ion translocation. In general, the $K_m = (k_1^- + k_2)/k_1^+$ and the dissociation constant $K_d = k_1^-/k_1^+$ should be identical, if k_2 has an insignificantly small value ($k_2 \ll k_1^-$). If instead ion translocation rather (norm.) than binding is observed, mostly a significant k_2 value results in a K_m value larger than the K_d. By plotting the normalized peak currents against the respective ion concentrations (Fig. 5, d–g) and fitting with the Michaelis–Menten equation, the K_m values of KtrB for Na^+, K^+, Rb^+, and Cs^+ were determined. Peak currents obtained on one sensor chip were normalized against the highest current measured, allowing the merge of independently performed experiments with varying reconstitution efficiencies and/or liposome associations to the SSM. The obtained K_m value for Cs^+ (2.1 mM) is similar to its K_d value of 1.7 mM (Fig. 4 g and Table 1). With 5.9 mM, the K_m for Rb^+ is slightly increased compared with its K_d of 2.4 mM (Fig. 4 f and Table 1). For Na^+, a K_m of 35.5 mM was determined (Fig. 4 d and Table 1), which to some extent may reflect a very low binding affinity not detectable with the performed ITC measurements. With 16.4 mM, the K_m value of K^+ is significantly higher than the respective apparent K_d value of 91 µM (compare Fig. 3 b, Fig. 5 e, and Table 1). The increased K_m values suggest that K^+ and to a lesser extent Rb^+ are translocated through KtrB, while Cs^+ probably only binds. Whether Na^+ is indeed translocated remained unclear. Consequently, by the use of SSM-based electrophysiology, only K^+ was unambiguously identified as being translocated, while the results for Na^+ and Rb^+ were inconclusive. Cs^+, however, seemed to only bind to KtrB.

One could argue that the high K_m value of 16.4 mM determined for potassium is again a result of the lack of small ions in the buffer. To test this hypothesis, we repeated the SSM-based electrophysiology measurements with different KCl concentrations in the presence of 5 mM NaCl. However, the ion translocation did not change in comparison to the absence of Na^+, as demonstrated by similar decay times (τ_2 = 14.8 ms vs. 15.2 ms) and K_m values (28.9 mM vs. 16.4 mM; compare Fig. 5, e and h). This observation was supported by KtrB-mediated whole-cell potassium uptake measurements. For those, *ktrB* was expressed in *E. coli* strain LB2003, which lacks all major endogenous potassium uptake systems, allowing the determination of KtrB-mediated K^+ uptake into cation-depleted cells. In the absence of Na^+, K^+ uptake was determined with a V_{max} of 44.9 nmol·min^{-1}·mg^{-1} and a K_m of 2.9 mM by recording uptake traces at four different KCl concentrations (Fig. 6, a and b). In agreement with the performed SSM-based electrophysiology, the uptake traces did not change in the presence of increasing sodium ion concentrations (Fig. 6 c). In conclusion, Na^+ appears to modulate the selectivity filter of KtrB, leading to the highly selective binding of potassium ions. The sequential ion translocation via KtrB is not affected by Na^+ but is restricted by a

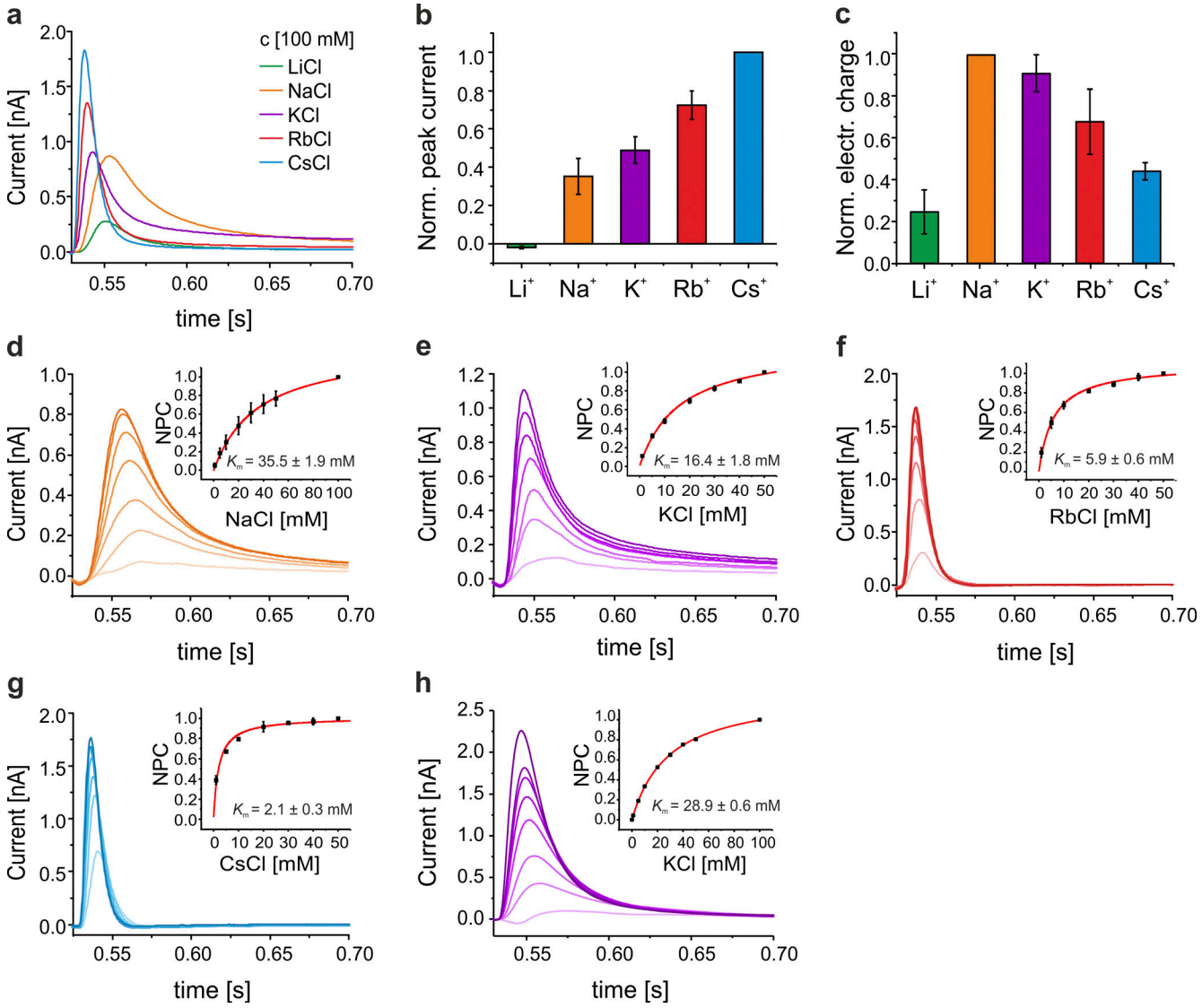

Figure 5. **Ion specificity of electrogenic behavior of KtrB analyzed using SSM-based electrophysiology.** The results of the SSM-based experiments for the cations Li^+, Na^+, K^+, Rb^+, and Cs^+ are shown in green, orange, purple, red, and blue, respectively. **(a)** Transient currents induced by 100 mM concentration jumps of LiCl, NaCl, KCl, RbCl, and CsCl on one sensor. **(b)** Bar graph of the peak currents in panel a performed experiments normalized to the highest peak current (CsCl). All data are corrected by subtraction of empty liposome signals (±SEM, n = 3). **(c)** Bar graph of integrated transient currents (0.52–1 s) normalized to the biggest area (Na^+). The normalized electrical (norm. electr.). charges were 0.25 ± 0.11 for Li^+, 1 for Na^+, 0.91 ± 0.09 for K^+, 0.68 ± 0.16 for Rb^+, and 0.44 ± 0.04 for Cs^+. All data are corrected by subtraction of empty liposome signals (±SEM, n = 3). **(d–g)** Concentration jumps with increasing salt concentrations are indicated by rising color intensities (1–50 or 100 mM). All data were corrected by subtraction of empty liposome signals. For determining the K_m values with OriginPro2017, peak currents were normalized (NPC) to the highest concentration jump during one set of measurements (±SEM, $n \geq 3$). The determined K_m values are 35.5 ± 1.9 mM for Na^+ (d), 16.4 ± 1.8 mM for K^+ (e), 5.9 ± 0.6 mM for Rb^+ (f), and 2.1 ± 0.3 mM for Cs^+ (g). **(h)** Concentration jumps with increasing KCl concentrations (1–100 mM) in the presence of 5 mM NaCl in the SSM buffer are shown. For K_m evaluation, peak currents were normalized (NPC) to the 100 mM concentration jump and fitted with OriginPro 2017.

secondary rate-limiting step, as indicated by the increased K_m values in comparison to the apparent K_d values.

Size-dependent ion translocation and the role of the intramembrane loop

The SSM-based electrophysiology measurements on KtrB-containing liposomes suggested the translocation of K^+ and to some extent of Na^+ and Rb^+, while particularly Cs^+ appeared to only bind. However, it remained challenging to discriminate between contributions of binding and translocation. Consequently, we were in need of another in vitro assay, which exclusively relies on ion translocation. For this, we established ACMA-based flux measurements (Su et al., 2016; Fig. 5). Liposomes with and without KtrB loaded with Na^+, K^+, Rb^+, or Cs^+ were diluted into Li^+-containing buffer, which established a gradient for the internal ion over the membrane. Ion efflux was initiated by the addition of H^+ ionophore CCCP, which permitted the influx of H^+ for every cation leaving the liposome. This setup has two advantages. First, the H^+ influx can be easily monitored by measuring H^+-dependent quenching of ACMA as an indirect

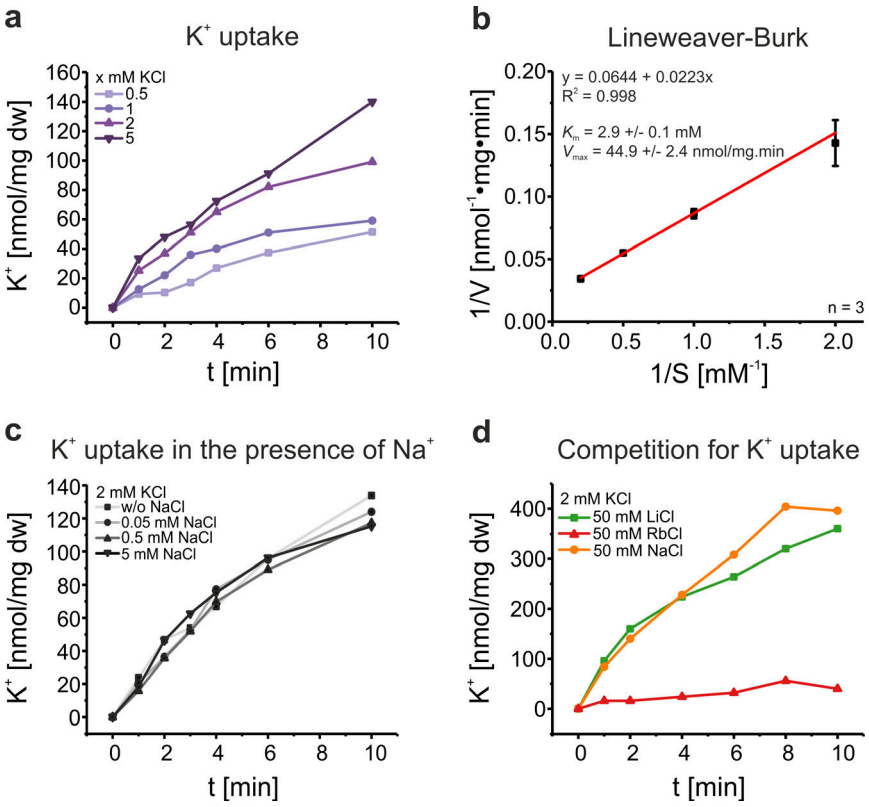

Figure 6. **K⁺ uptake by *E. coli* cells containing KtrB.** The strain LB2003/pEL901 was grown and induced for *ktrB* expression with 0.02% L-arabinose. For the K⁺ uptake experiment, cells were suspended to 1 mg dry weight (dw)/ml of medium containing 200 mM HEPES-triethanolamin, pH 7.5, 0.2% glycerol, and 0.02% L-arabinose. The suspension was shaken at room temperature. **(a)** After 10 min, KCl was added at the following concentrations: 0.5 mM, 1 mM, 2 mM, and 5 mM. For each data point, a 1.0-ml sample was taken from the suspension and centrifuged through silicone oil, and the cellular K⁺ content was determined by flame photometry. **(b)** Triplicates of panel a were used to determine K_m and V_{max} values applying a Lineweaver–Burk plot. **(c)** K⁺ uptake using 2 mM KCl in the presence of the following NaCl concentrations was examined: 0 mM, 0.05 mM, 0.5 mM, and 5 mM. **(d)** K⁺ uptake using 2 mM KCl in the presence of competitive ion concentrations was examined using 50 mM NaCl or RbCl; 50 mM LiCl was used as a noncompetitive ion.

readout for cation efflux. Second, H^+ influx counteracts charge buildup caused by cation efflux, permitting continued cation efflux. As expected, liposomes without KtrB showed hardly any effect upon addition of CCCP, while the further addition of Val (as ionophore for K^+, Rb^+, and Cs^+) or Na^+ ionophore IV (as ionophore for Na^+) abolished the established gradients leading to ACMA quenching. Similarly, the addition of CCCP to KtrB-containing liposomes loaded with Cs^+ did not result in any fluorescence decrease. Surprisingly, the fastest quenching was observed for Na^+-loaded proteoliposomes followed by those loaded with K^+. Instead, the presence of Rb^+ caused only poor quenching, indicating very slow ion fluxes (Fig. 7). In summary, the ACMA-based flux assay with liposome-reconstituted wild-type KtrB qualitatively disclosed a size-dependent permeability of KtrB for the tested cations ($Na^+ > K^+ >> Rb^+ >>> Cs^+$).

In the next step, we aimed to elucidate the basis for the size-dependent ion fluxes. Based on published data (Hänelt et al., 2010a,b; Vieira-Pires et al., 2013; Diskowski et al., 2017) it was plausible to speculate that ion fluxes are restricted by the intramembrane loop (Fig. 1), which has been shown to act as a molecular gate in KtrB. We hypothesized that it might serve as a barrier for the bigger ions K^+, Rb^+, and Cs^+ as it narrows the pore size just below the selectivity filter, while Na^+ might just slip through. To test this hypothesis, we used previously characterized variants of KtrB with mutations in the intramembrane loop (Hänelt et al., 2010a). In whole-cell uptake assays, these variants showed increased V_{max} values for K^+, while the K_m as well as the uptake of Na^+ remained unchanged. In vivo, the most severe effects were seen upon the complete deletion of the intramembrane loop. Unfortunately, those variants appeared to precipitate upon purification. Instead, we performed the ACMA-based flux assay with variant $KtrB_{G316S}$, which in the in vivo measurements showed an approximately fourfold increased V_{max} for K^+ uptake compared with wild-type KtrB. In the ACMA-based flux assay, this variant showed extremely fast K^+ fluxes, followed by Rb^+ and Na^+, while Cs^+ still remained impermeable (Fig. 7 c). With approximately 10 ms^{-1}, the decay rates ($k = 1/t_1$) of the fluorescence quenching attributed to Na^+ fluxes were comparable to those of wild-type KtrB-containing liposomes (Fig. 7 d). In contrast, the decay rates reflecting Rb^+ and K^+ fluxes were increased by a factor of 8 (1.6 ms^{-1} vs. 12.6 ms^{-1}) and by a factor of 60 (1.6 ms^{-1}–100 ms^{-1}), respectively. In conclusion, the intact intramembrane loop in fact appears to hinder the faster fluxes of K^+ and Rb^+ ions matching with its proposed role as channel gate. Single amino acid mutations within the intramembrane loop are sufficient to disturb the gating, leading to an increased open probability or even the less efficient closing of the channel. In contrast, Na^+ fluxes seem not to interfere with the intramembrane loop, as confirmed by our in vitro and previous in vivo studies (Hänelt et al., 2010a). Whether Cs^+ would ever permeate through KtrB or whether it only binds to the selectivity filter remains unknown.

The role of Na^+ in K^+ uptake by the KtrAB complex

Based on the attempts so far, Na^+ appears to have two roles in KtrB. On the one hand, at high concentrations, Na^+ is an efficiently translocated substrate. On the other hand, already at lower concentrations, Na^+ seems to bind somewhere in KtrB, which leads to a significantly increased affinity for K^+ over all other tested cations. Under physiological conditions, Na^+ is

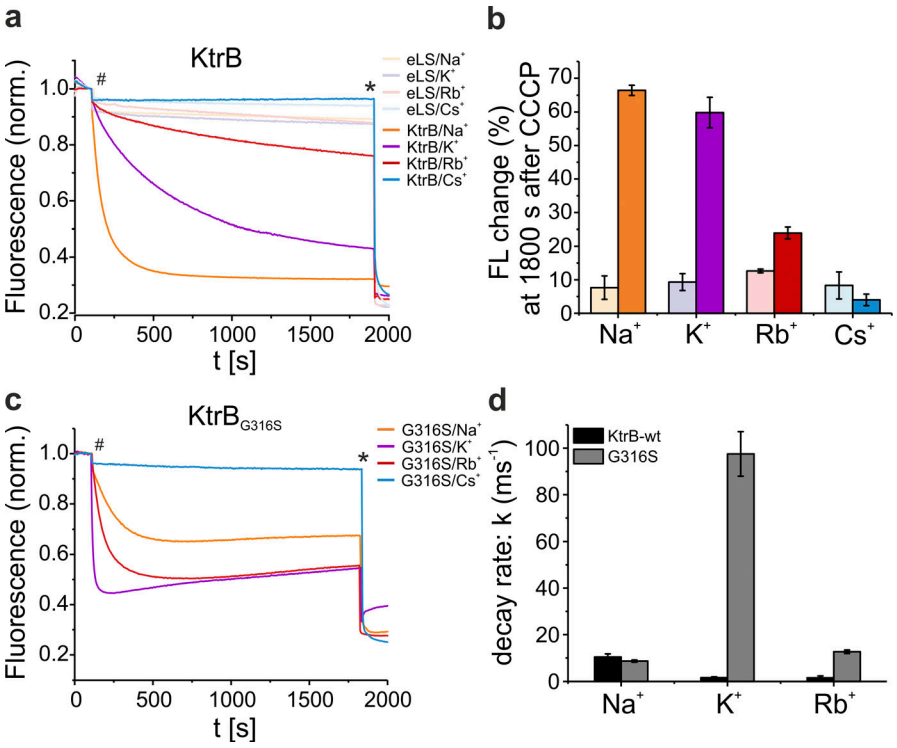

Figure 7. **Ion permeability determined by ACMA-based cation flux assay. (a)** KtrB-containing liposomes at an LPR of 100:1 loaded with NaCl (orange), KCl (purple), RbCl (red), or CsCl (blue) were diluted 1:20 into LiCl-based buffer. Empty liposomes filled with the respective cations are shown as a control (light colors). The addition of H^+ ionophore CCCP is indicated by the number sign (#). Consequently, the efflux of ions was accompanied by an intravesicular pH decrease, which quenched the fluorescent dye ACMA. Finally, for the normalization (norm.) of all data, sodium ionophore IV (NaI IV) for NaCl-containing liposomes or Val for all other intravesicular cations was added, indicated by the asterisk (*). This induced protein-independent cation efflux leading to maximal ACMA quenching. **(b)** Fluorescence (FL) change (%) of proteoliposomes and empty liposomes at 1,800 s after CCCP addition are shown in a bar graph ($n \geq 3$, ±SD). **(c)** $KtrB_{G316S}$-containing liposomes at an LPR of 100:1 loaded with NaCl (orange), KCl (purple), RbCl (red), or CsCl (blue) were diluted 1:20 into LiCl-based buffer. Experiments were performed as described above. **(d)** Decay rates ($k = 1/t_1$) for one-phase exponential decays ($y = y_0 + A^{-k}t$) of Na^+, K^+, and Rb^+ fluxes mediated by wild-type (wt) KtrB and $KtrB_{G316S}$, respectively, are shown in a bar graph ($n \geq 3$, ±SD).

usually present in great excess over K^+. Yet K^+ should preferentially be taken up to act in osmoprotection. Until now, both our in vitro and our in vivo transport approaches covered single ion conditions only, while mixed ion conditions cannot be evaluated with the in vitro approaches. However, ITC measurements with K^+ in the presence of high concentrations of Na^+ suggested a preferred binding of K^+ over Na^+ by revealing a K_d value in a low millimolar range. To determine whether the preferred K^+ binding also results in the selective translocation of K^+, we performed another set of whole-cell potassium uptake measurements in the presence of an excess of Li^+, Na^+, and Rb^+, respectively. Since previous experiments showed that Li^+ neither binds to nor is translocated by KtrB, the uptake of K^+ (2 mM added to the outside buffer) in the presence of 50 mM LiCl served as a positive control. In the presence of 50 mM NaCl, K^+ uptake was similar to the positive control, while 50 mM RbCl efficiently inhibited the uptake of potassium ions (Fig. 6 d). Thus, the high affinity of KtrB toward potassium, which results from the presence of Na^+ itself, appears to be sufficient to favor the uptake of potassium over sodium ions as required. Rb^+ binds with significantly higher affinity than Na^+ and remarkably reduces K^+ uptake. However, Rb^+ is not physiologically relevant.

In all the experiments shown so far, the regulatory subunit KtrA was missing. Based on present structural data, it seems plausible that KtrA does not affect the initial ion selectivity provided by the selectivity filter. Yet it is involved in regulating gating by the intramembrane loop. ATP binding to KtrA was hypothesized to favor the activated conformation of KtrB while ADP binding stabilizes the loop in a closed conformation (Szollosi et al., 2016; Diskowski et al., 2017). Additionally, the activity of the KtrAB complex has long been known to depend on the presence of Na^+ in vivo; in its absence, only poor K^+ uptake was determined (Tholema et al., 1999). This observation suggests that Na^+ binding to the complex is also involved in the regulating of the gating. To detail the role of Na^+ on the KtrAB system, we would have preferred to apply the in vitro assays established here. However, until now, we have not been able to establish a purification and reconstitution protocol for the functionally assembled complex. Instead, a sandwiched complex of an octameric ring of KtrA wedged in between two KtrB dimers has always been found (Diskowski et al., 2017). Alternatively, we performed another series of whole-cell K^+ uptake experiments, in which the uptake of K^+ through KtrAB was determined at four different K^+ concentrations (0.5, 1, 2, and 5 mM) in the presence of four different Na^+ concentrations (0, 0.05, 0.5, and 5 mM) each. A comparison of the raw traces already showed significantly increased uptake rates upon increasing the Na^+ concentration (Fig. 8 a). The analysis of the Michaelis–Menten kinetics revealed that upon increased Na^+ concentration, the V_{max} increased more than twofold (from 29 $nmol \cdot min^{-1} \cdot mg^{-1}$ in the absence of Na^+ to 66 $nmol \cdot min^{-1} \cdot mg^{-1}$ in the presence of 5 mM Na^+), while at the same time the K_m drastically decreased more than 20-fold from 1 mM to 37 µM (Fig. 8, b and c). In the absence of Na^+, the KtrAB complex showed similar kinetics to the KtrB subunit alone (compare Fig. 6, a and b; and Fig. 8), while the presence of physiological concentrations of Na^+ significantly facilitated the uptake of K^+. Thus, within the KtrAB complex, Na^+ not only modulates the selectivity filter toward higher affinities for K^+ but also controls the rate-limiting step, the gating, probably by stabilizing the active, open conformation of the channel.

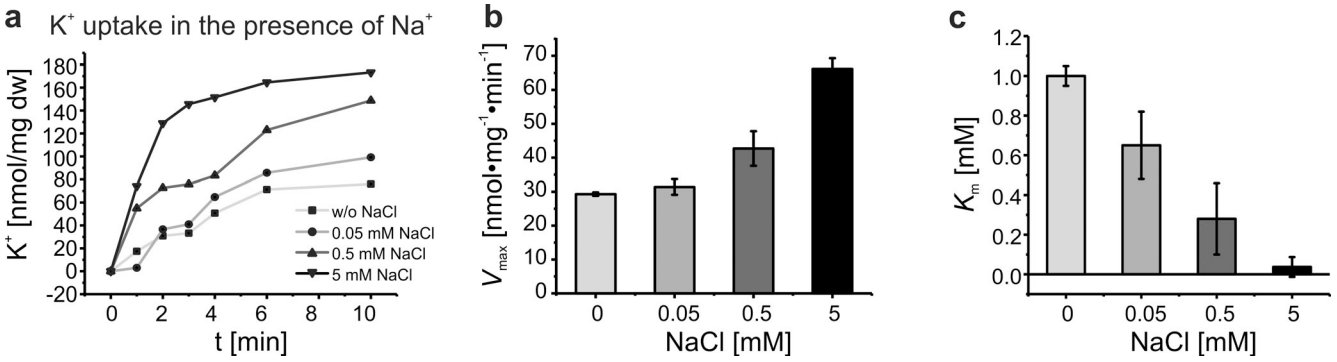

Figure 8. **K⁺ uptake by *E. coli* cells containing KtrAB.** The strain LB2003/pKT84 was grown and induced for *ktrAB* expression with 0.02% L-arabinose. For the K^+ uptake experiment, cells were suspended to 1 mg dry weight (dw)/ml of medium containing 200 mM HEPES-triethanolamin, pH 7.5, 0.2% glycerol, and 0.02% L-arabinose. The suspension was shaken at room temperature. **(a)** After 10 min, 2 mM KCl was added in the presence of the following NaCl concentrations: 0 mM, 0.05 mM, 0.5 mM, and 5 mM. For each data point, a 1.0-ml sample was taken from the suspension and centrifuged through silicone oil, and the cellular K^+ content was determined by flame photometry. **(b and c)** K^+ uptake experiments at different KCl concentrations in the presence of different NaCl concentrations were performed in triplicate. Subsequently, K_m and V_{max} dependent on different NaCl concentration were determined (n = 3, ±SD).

Discussion

The selectivity filter of KtrB is poorly conserved in comparison to tetrameric potassium channels, which harbor the T(X)GYG motif or slight variation thereof (Durell and Guy, 1999; Hänelt et al., 2011). It is generally believed that with only one conserved glycine residue per P-loop, KtrB and its homologue TrkH have to be unselective for alkali metal cations (Cao et al., 2013). This would be in agreement with previous studies on K^+ channels with a canonical selectivity filter, which showed decreased ion selectivity when either the selectivity filter's or the pore region's sequence conservation was decreased (Cheng et al., 2011; Furini and Domene, 2013; Sauer et al., 2013). However, such unspecific behavior would contradict KtrAB's suggested function as a selective K^+ uptake system for ion homeostasis. Here we demonstrate that KtrB is in fact more selective in ion binding and translocation than anticipated. KtrB binds K^+ with high affinity compared with all other tested cations. This high binding affinity depends on the presence of small cations such as Li^+ and Na^+, but it remains elusive how they modulate the selectivity filter and alter the binding affinities. In fact, the apparent K_d value for K^+ in the presence of Li^+ is similar to the affinities determined for other K^+ channels, which are either K^+-selective when bearing the canonical selectivity filter TVGYG (Lockless et al., 2007) or are nonselective with the corresponding sequence of TVGDG as found in NaK channels (Lockless et al., 2007; Liu et al., 2012). Mutational studies on NaK channels showed that not only the equilibrium ion preference but also the number of high-affinity binding sites are crucial for a selective K^+ channel (Liu and Lockless, 2013; Sauer et al., 2013). A general double barrier mechanism was proposed to explain K^+ selectivity at low K^+ concentrations (Sauer et al., 2013). Since at increased Na^+ concentrations the K^+ translocation through KtrB was shown not to be affected, KtrB qualifies as a selective K^+ channel. If selectivity in KtrB follows the double barrier mechanism, it should thus have at least three ion binding sites, allowing the binding of two K^+ ions at a time. In the structures of KtrB and TrkH, only a single K^+ was identified in the S3 binding site of the selectivity filters (Cao et al., 2011; Vieira-Pires et al., 2013). However, MD simulations on TrkH proposed the existence of two to three additional binding sites (Domene and Furini, 2012). Here, the small cations Li^+ and, more importantly, Na^+ could play an essential role. Based on our data, we hypothesize that small cations significantly modulate the selectivity filter, which leads to the observed increased affinity for potassium ions but which might also contribute to the stabilization of additional binding sites. If this is the case, the role of small cations might be different in TrkH, which could explain the differences in ion selectivity between KtrAB and TrkAH (Cao et al., 2013). Although structurally very similar (Cao et al., 2011; Vieira-Pires et al., 2013), a comparable Na^+ dependency has not been described for Trk(A)H. However, comparable studies on ion binding are missing for TrkH, so we cannot exclude that Li^+ and Na^+ would similarly increase the K^+ binding affinity.

A motif exclusive to KtrB and TrkH is the intramembrane loop, which was previously suggested to function as a gate (Hänelt et al., 2010a,b; Vieira-Pires et al., 2013; Diskowski et al., 2017). Our data elucidate that the intramembrane loop significantly limits ion translocation of K^+ and Rb^+, serving as a second layer of regulation in KtrB. The translocation of the smaller Na^+ is not impaired by the gate. In the absence of the regulatory subunit KtrA, the open probability of the gate seems to be limited, resulting in slow K^+ and very slow Rb^+ fluxes. Interestingly, in the presence of KtrA, Na^+ appears to affect gating. It previously was shown to increase the uptake velocity for K^+ (Tholema et al., 2005). Here we elucidated that Na^+ also decreases the K_m value of K^+ translocation, approaching the K_d of K^+ binding. Consequently, under this condition, rate constant k_2 is insignificantly small, and the K^+ binding seems to limit ion translocation, suggesting the stabilization of the open conformation of the gate. It remains elusive where sodium can bind. One possibility is that Na^+ binds to the regulatory KtrA subunit as shown for other regulators of K^+ conductance domains, which are activated by Na^+ (Hite et al., 2015). Alternatively, Na^+ could exclusively bind to KtrB, as observed by the increased K^+ binding affinity in its presence. Due to the close proximity of the gating area and the selectivity filter, this may then result in a synergistic

effect between the Na^+ binding to KtrB and the regulatory effect of KtrA.

Acknowledgments

Richard W. Aldrich served as editor.

We thank Dr. Dorith Wunnicke for critically reading the manuscript, Dr. Andre Bazzone for helpful discussions, and Prof. Dr. Jens Wöhnert for providing access to the MicroCal iTC200 System.

This work was supported by the Max Planck Society (K. Fendler) and by the German Research Foundation via Emmy Noether grants HA 6322/3-1 (I. Hänelt), HA 6322/2-1 (I. Hänelt), and SFB 807 Membrane Transport and Communication (K. Fendler and I. Hänelt).

The authors declare no competing financial interests.

Author contributions: V. Mikušević and I. Hänelt conceived the project. V. Mikušević performed most of the experiments. M. Schrecker performed some ITC measurements and helped with the establishment of the purification protocol; N. Kolesova performed some whole-cell uptake assays. M. Patiño-Ruiz and K. Fendler taught V. Mikušević the use of SSM-based electrophysiology and helped with data interpretation. V. Mikušević and I. Hänelt interpreted the data and wrote the manuscript. All authors proofread the manuscript. K. Fendler and I. Hänelt supervised work and acquired funding.

Submitted: 18 April 2019
Revised: 3 September 2019
Accepted: 27 September 2019

References

Bakker, E.P., and W.E. Mangerich. 1983. The effects of weak acids on potassium uptake by *Escherichia coli* K-12 inhibition by low cytoplasmic pH. *Biochim. Biophys. Acta.* 730:379–386. https://doi.org/10.1016/0005-2736(83)90355-3

Bazzone, A., W.S. Costa, M. Braner, O. Călinescu, L. Hatahet, and K. Fendler. 2013. Introduction to solid supported membrane based electrophysiology. *J. Vis. Exp.* 75:e50230.

Bazzone, A., M.G. Madej, H.R. Kaback, and K. Fendler. 2016. pH Regulation of Electrogenic Sugar/H^+ Symport in MFS Sugar Permeases. *PLoS One.* 11: e0156392. https://doi.org/10.1371/journal.pone.0156392

Bazzone, A., A.J. Zabadne, A. Salisowski, M.G. Madej, and K. Fendler. 2017. A Loose Relationship: Incomplete H^+/Sugar Coupling in the MFS Sugar Transporter GlcP. *Biophys. J.* 113:2736–2749. https://doi.org/10.1016/j.bpj.2017.09.038

Cao, Y., X. Jin, H. Huang, M.G. Derebe, E.J. Levin, V. Kabaleeswaran, Y. Pan, M. Punta, J. Love, J. Weng, et al. 2011. Crystal structure of a potassium ion transporter, TrkH. *Nature.* 471:336–340. https://doi.org/10.1038/nature09731

Cao, Y., Y. Pan, H. Huang, X. Jin, E.J. Levin, B. Kloss, and M. Zhou. 2013. Gating of the TrkH ion channel by its associated RCK protein TrkA. *Nature.* 496:317–322. https://doi.org/10.1038/nature12056

Cheng, W.W., J.G. McCoy, A.N. Thompson, C.G. Nichols, and C.M. Nimigean. 2011. Mechanism for selectivity-inactivation coupling in KcsA potassium channels. *Proc. Natl. Acad. Sci. USA.* 108:5272–5277. https://doi.org/10.1073/pnas.1014186108

Diskowski, M., V. Mikusevic, C. Stock, and I. Hänelt. 2015. Functional diversity of the superfamily of K^+ transporters to meet various requirements. *Biol. Chem.* 396:1003–1014. https://doi.org/10.1515/hsz-2015-0123

Diskowski, M., A.R. Mehdipour, D. Wunnicke, D.J. Mills, V. Mikusevic, N. Bärland, J. Hoffmann, N. Morgner, H.J. Steinhoff, G. Hummer, et al. 2017. Helical jackknives control the gates of the double-pore K^+ uptake system KtrAB. *eLife.* 6:e24303. https://doi.org/10.7554/eLife.24303

Domene, C., and S. Furini. 2012. Molecular dynamics simulations of the TrkH membrane protein. *Biochemistry.* 51:1559–1565. https://doi.org/10.1021/bi201586n

Doyle, D.A., J. Morais Cabral, R.A. Pfuetzner, A. Kuo, J.M. Gulbis, S.L. Cohen, B.T. Chait, and R. MacKinnon. 1998. The structure of the potassium channel: molecular basis of K^+ conduction and selectivity. *Science.* 280: 69–77. https://doi.org/10.1126/science.280.5360.69

Driessen, A.J.M., and W.N. Konings. 1993. Insertion of lipids and proteins into bacterial membranes by fusion with liposomes. *Methods Enzymol.* 221: 394–408. https://doi.org/10.1016/0076-6879(93)21032-4

Durell, S.R., and H.R. Guy. 1999. Structural models of the KtrB, TrkH, and Trk1,2 symporters based on the structure of the KcsA $K(^+)$ channel. *Biophys. J.* 77:789–807. https://doi.org/10.1016/S0006-3495(99)76932-8

Epstein, W. 2003. The roles and regulation of potassium in bacteria. *Prog. Nucleic Acid Res. Mol. Biol.* 75:293–320. https://doi.org/10.1016/S0079-6603(03)75008-9

Furini, S., and C. Domene. 2013. $K(^+)$ and $Na(^+)$ conduction in selective and nonselective ion channels via molecular dynamics simulations. *Biophys. J.* 105:1737–1745. https://doi.org/10.1016/j.bpj.2013.08.049

Garcia-Celma, J.J., L. Hatahet, W. Kunz, and K. Fendler. 2007. Specific anion and cation binding to lipid membranes investigated on a solid supported membrane. *Langmuir.* 23:10074–10080. https://doi.org/10.1021/la701188f

Geertsma, E.R., N.A. Nik Mahmood, G.K. Schuurman-Wolters, and B. Poolman. 2008. Membrane reconstitution of ABC transporters and assays of translocator function. *Nat. Protoc.* 3:256–266. https://doi.org/10.1038/nprot.2007.519

Gundlach, J., C. Herzberg, V. Kaever, K. Gunka, T. Hoffmann, M. Weiß, J. Gibhardt, A. Thürmer, D. Hertel, R. Daniel, et al. 2017. Control of potassium homeostasis is an essential function of the second messenger cyclic di-AMP in *Bacillus subtilis*. *Sci. Signal.* 10:eaal3011. https://doi.org/10.1126/scisignal.aal3011

Hänelt, I., S. Löchte, L. Sundermann, K. Elbers, M. Vor der Brüggen, and E.P. Bakker. 2010a. Gain of function mutations in membrane region M2C2 of KtrB open a gate controlling K^+ transport by the KtrAB system from *Vibrio alginolyticus*. *J. Biol. Chem.* 285:10318–10327. https://doi.org/10.1074/jbc.M109.089870

Hänelt, I., D. Wunnicke, M. Müller-Trimbusch, M. Vor der Brüggen, I. Kraus, E.P. Bakker, and H.J. Steinhoff. 2010b. Membrane region M2C2 in subunit KtrB of the K^+ uptake system KtrAB from *Vibrio alginolyticus* forms a flexible gate controlling K^+ flux: an electron paramagnetic resonance study. *J. Biol. Chem.* 285:28210–28219. https://doi.org/10.1074/jbc.M110.139311

Hänelt, I., N. Tholema, N. Kröning, M. Vor der Brüggen, D. Wunnicke, and E.P. Bakker. 2011 KtrB, a member of the superfamily of K^+ transporters. *Eur. J. Cell Biol.* 90:696–704. https://doi.org/10.1016/j.ejcb.2011.04.010

Hille, B. 2001. *Ionic channels of excitable membranes.* Sinauer Associates, Sunderland, Massachusetts. 814 pp.

Hite, R.K., P. Yuan, Z. Li, Y. Hsuing, T. Walz, and R. MacKinnon. 2015 Cryo-electron microscopy structure of the Slo2.2 Na(+)-activated K(+) channel. *Nature.* 527:198–203. https://doi.org/10.1038/nature14958

Holtmann, G., E.P. Bakker, N. Uozumi, and E. Bremer. 2003. KtrAB and KtrCD: two K^+ uptake systems in *Bacillus subtilis* and their role in adaptation to hypertonicity. *J. Bacteriol.* 185:1289–1298. https://doi.org/10.1128/JB.185.4.1289-1298.2003

Krishnan, M.N., J.P. Bingham, S.H. Lee, P. Trombley, and E. Moczydlowski. 2005. Functional role and affinity of inorganic cations in stabilizing the tetrameric structure of the KcsA K^+ channel. *J. Gen. Physiol.* 126:271–283. https://doi.org/10.1085/jgp.200509323

Kröning, N., M. Willenborg, N. Tholema, I. Hänelt, R. Schmid, and E.P. Bakker. 2007. ATP binding to the KTN/RCK subunit KtrA from the K^+-uptake system KtrAB of *Vibrio alginolyticus*: its role in the formation of the KtrAB complex and its requirement in vivo. *J. Biol. Chem.* 282: 14018–14027. https://doi.org/10.1074/jbc.M609084200

Levin, E.J., and M. Zhou. 2014. Recent progress on the structure and function of the TrkH/KtrB ion channel. *Curr. Opin. Struct. Biol.* 27:95–101. https://doi.org/10.1016/j.sbi.2014.06.004

Liu, S., and S.W. Lockless. 2013. Equilibrium selectivity alone does not create K^+-selective ion conduction in K^+ channels. *Nat. Commun.* 4:2746. https://doi.org/10.1038/ncomms3746

Liu, S., X. Bian, and S.W. Lockless. 2012. Preferential binding of K^+ ions in the selectivity filter at equilibrium explains high selectivity of K^+ channels *J. Gen. Physiol.* 140:671–679. https://doi.org/10.1085/jgp.201210855

Lockless, S.W., M. Zhou, and R. MacKinnon. 2007. Structural and thermodynamic properties of selective ion binding in a K^+ channel. *PLoS Biol.* 5: e121. https://doi.org/10.1371/journal.pbio.0050121

Lundberg, M.E., E.C. Becker, and S. Choe. 2013. MstX and a putative potassium channel facilitate biofilm formation in *Bacillus subtilis*. *PLoS One.* 8: e60993. https://doi.org/10.1371/journal.pone.0060993

Prindle, A., J. Liu, M. Asally, S. Ly, J. Garcia-Ojalvo, and G.M. Süel. 2015. Ion channels enable electrical communication in bacterial communities. *Nature.* 527:59–63. https://doi.org/10.1038/nature15709

Sauer, D.B., W. Zeng, J. Canty, Y. Lam, and Y. Jiang. 2013. Sodium and potassium competition in potassium-selective and non-selective channels. *Nat. Commun.* 4:2721. https://doi.org/10.1038/ncomms3721

Schulz, P., J.J. Garcia-Celma, and K. Fendler. 2008. SSM-based electrophysiology. *Methods.* 46:97–103. https://doi.org/10.1016/j.ymeth.2008.07.002

Stumpe, S., and E.P. Bakker. 1997. Requirement of a large K^+-uptake capacity and of extracytoplasmic protease activity for protamine resistance of *Escherichia coli*. *Arch. Microbiol.* 167:126–136. https://doi.org/10.1007/s002030050425

Su, Z., E.C. Brown, W. Wang, and R. MacKinnon. 2016. Novel cell-free high-throughput screening method for pharmacological tools targeting K^+ channels. *Proc. Natl. Acad. Sci. USA.* 113:5748–5753. https://doi.org/10.1073/pnas.1602815113

Szollosi, A., R.S. Vieira-Pires, C.M. Teixeira-Duarte, R. Rocha, and J.H. Morais-Cabral. 2016. Dissecting the Molecular Mechanism of Nucleotide-Dependent Activation of the KtrAB K^+ Transporter. *PLoS Biol.* 14: e1002356. https://doi.org/10.1371/journal.pbio.1002356

Tholema, N., E.P. Bakker, A. Suzuki, and T. Nakamura. 1999. Change to alanine of one out of four selectivity filter glycines in KtrB causes a two orders of magnitude decrease in the affinities for both K^+ and Na^+ of the Na^+ dependent K^+ uptake system KtrAB from *Vibrio alginolyticus*. *FEBS Lett.* 450:217–220. https://doi.org/10.1016/S0014-5793(99)00504-9

Tholema, N., M. Vor der Brüggen, P. Mäser, T. Nakamura, J.I. Schroeder, H. Kobayashi, N. Uozumi, and E.P. Bakker. 2005. All four putative selectivity filter glycine residues in KtrB are essential for high affinity and selective K^+ uptake by the KtrAB system from *Vibrio alginolyticus*. *J. Biol. Chem.* 280:41146–41154. https://doi.org/10.1074/jbc.M507647200

Vieira-Pires, R.S., A. Szollosi, and J.H. Morais-Cabral. 2013. The structure of the KtrAB potassium transporter. *Nature.* 496:323–328. https://doi.org/10.1038/nature12055

Williams, R.J., and E.C. Wacker. 1967. Cation balance in biological systems. *JAMA.* 201:96–100. https://doi.org/10.1001/jama.201.1.96